# Angle dependence of the interface magnetic configuration in a model antiferromagnetically coupled ferrimagnetic/ferrimagnetic bilayer GdFe/TbFe

Stéphane Mangin, Luc Thomas, Francois Montaigne, Weiwei Lin, Thomas Hauet, Y Henry

# Angle dependence of the interface magnetic configuration in a model antiferromagnetically coupled ferrimagnetic/ferrimagnetic bilayer GdFe/TbFe

S. Mangin,[1,*] L. Thomas,[2,3] F. Montaigne,[1] W. Lin,[1] T. Hauet,[1] and Y. Henry[4]
[1]*Institut Jean Lamour, UMR CNRS 7198–Nancy Université, BP 70239, F-54506 Vandoeuvre, France*
[2]*IBM Research Division, Almaden Research Center, San Jose, California 95120, USA*
[3]*Groupe d'étude de la matière condensée, UMR CNRS 8635, Université de Versailles Saint Quentin, 78035 Versailles Cedex, France*
[4]*IPCMS, UMR CNRS 7504, Université Louis Pasteur, F-67034 Strasbourg Cedex 2, France*
(Received 4 September 2009; revised manuscript received 20 October 2009; published 28 December 2009)

The evolution of the magnetic configuration inside an antiferromagnetically coupled GdFe/TbFe bilayer is studied at room temperature. For such system exchange-bias behaviors have been previously reported and are found to depend on the magnetic configuration above the blocking temperature (~250 K). Here, the in-plane components of the magnetization are studied for different applied-field orientations. By comparing those results with a one-dimensional micromagnetic model the evolution of the interface magnetic configuration is well described. For the different applied-field orientations the magnetic behavior is found to be dominated by the formation of a magnetic twist at the interface which may adopt one chirality or the other.

DOI: 10.1103/PhysRevB.80.224424 PACS number(s): 75.70.Cn, 75.60.Ch, 75.60.Jk

## I. INTRODUCTION

Understanding and tailoring exchange bias are still subjects of interest in magnetism, especially because it allows controlling the magnetization orientation of magnetic layers in spintronic devices.[1] It is now well established that a ferromagnetic coupling at the interface of ferromagnetic/antiferromagnetic (FM/AFM) systems[2–5] or hard/soft "spring magnets" bilayers[6,7] can lead to exchange bias fields ($H_E$). This exchange-bias phenomenon leads to a shift in field of the FM hysteresis loop in the case of (FM/AFM) or of the soft-layer hysteresis loop in the case of spring magnet. It has been shown that in the case of an antiferromagnetic interface coupling for large positive cooling field the hysteresis loop may be shifted along the positive field direction. This effect is referred usually to as positive exchange bias. Note that nevertheless it can give rise to a negative exchange-bias field if the sample is field cooled under certain condition. This phenomenon was first observed in FM/AFM systems as $Fe/FeF_2$ or $Fe/MnF_2$,[8] where the sample is cooled under a cooling field ($H_{fc}$) from a temperature above to a temperature below the blocking temperature $T_B$. $T_B$ is defined as the critical temperature at which exchange bias is observed and is found to be lower than the ordering Néel temperature ($T_N$) of the antiferromagnetic layer. A transition in $H_E$ from negative to positive with increasing cooling field ($H_{fc}$) values has been reported in Refs. 8–10. Two other phenomena were also evidenced: (i) an increase in the coercive field ($H_C$) as $H_E$ reaches zero and (ii) a shift of the hysteresis loop along the magnetization axis characterized by a magnetization shift $M_{Shift}$. How those phenomena are related to each other and the understanding of the magnetic interface configurations dependences on field and temperature is not fully understood and is still discussed in various bilayer systems.[11–13]

Very comparable behaviors were observed on a system that consists of an antiferromagnetic CoO layer exchange coupled to an antiferromagnetically coupled trilayer Co/Ru/Co (Ref. 14) or several rare-earth-based systems such as $DyFe_2/YFe_2$ (Refs. 13, 15, and 16) and $Gd_{40}Fe_{60}/Tb_{12}Fe_{88}$ bilayers in which the compositions have been chosen to obtain an antiferromagnetic interface coupling.[17–21] For this last system, it has been established that after having cooled the sample from room temperature to low temperature, the GdFe magnetically soft-layer hysteresis loop was shifted either toward a negative or a positive exchange-bias field depending on the $H_{fc}$ amplitude.[17] Also as in the FM/AFM system analogous $H_{fc}$ dependences of $H_C$ and $M_{Shift}$ are observed.[9] The advantage of the ferrimagnetic/ferrimagnetic systems over the "conventional" FM/AFM ones is that all layers have an average magnetization which can be measured. It is then much easier to deduce the magnetic configuration using rather simple techniques as magnetometry, magnetization ac susceptibility, and electrical-transport measurements.[22]

In the ferrimagnetic/ferrimagnetic systems, the cooling-field dependence of the exchange-bias phenomena was explained considering laterally uniform magnetization.[17] It was then demonstrated that the magnetic configuration which developed in the TbFe layer at room temperature is frozen at low temperature.[19,20] A blocking temperature $T_B$ may be defined around 250 K. Therefore the GdFe hysteresis loop is not shifted at room temperature. The exchange-bias-field value is found to be dominated by the angle between the magnetization of the interface TbFe layer and the cooling-field direction. The $M_{Shift}$ is given by the frozen interface magnetic configuration in the TbFe whereas $H_C$ is mostly related to magnetization reorganization at the interface in both layers when the GdFe-layer magnetization reverses.[21] Note that the exchange-bias properties depend on both the cooling-field amplitude and direction.[19] For a better understanding of exchange-bias phenomena and to study the effect of the cooling field on the final magnetic-interface configuration at low temperature, it is then of first interest to know which magnetic configurations prevail above $T_B$ and how those magnetic configurations evolved as the field (amplitude and direction) is changed.

The present paper is then devoted to study the magnetic configuration of antiferromagnetically coupled

 

$Gd_{40}Fe_{60}/Tb_{10}Fe_{90}$ at room temperature, i.e., above $T_B$. To obtain a reliable picture of the magnetic configuration in this system, we performed a set of magnetization measurements for different magnetic field directions and amplitudes, collecting both the longitudinal and transverse magnetization components. On the other hand we used a one-dimensional magnetization profile calculation which stable and metastable solutions are compared to experimental data. In the following the magnetization is assumed to be laterally uniform and only in depth magnetization variations are expected. This assumption has been previously verified using Neutron scattering[20] and Kerr microscopy.[21]

After a recall of the main characteristics of the GdFe/TbFe system and a presentation of the measurement procedure and the micromagnetic calculation (part II), we describe the experimental results and compare the data to those predicted by the calculation (part III). In this part, we deal successively with measurements performed with the magnetic field applied along the easy axis of the sample (III-1) along other directions (III-2) and then along the hard axis (III-3). Finally in Part IV, we conclude on the room-temperature magnetic configurations and their field dependence.

## II. SAMPLE AND EXPERIMENT

### A. GdFe/TbFe sample

For each of the two GdFe and TbFe alloys, the exchange magnetic coupling is positive between iron moments as well as between the rare-earth moments (Gadolinium and Terbium) but it is negative between the magnetic moments carried by iron and those carried by the rare earths. As a consequence, both alloys are ferrimagnetic with the iron moments in one direction and the rare earth ones in the opposite direction. Because of the local anisotropy, the magnetic rare-earth moments spread about their average direction.[23] The net magnetization inside each of these alloys depends on their compositions and can be along the rare-earth "subnet" magnetization or along the iron subnet magnetization.[24] This last case can take place only in very rich iron alloys because Fe carries a small magnetic moment (around $2\mu_B$) as compared to that of Gd or Tb (around $9\mu_B$).

The compositions of the alloys have been chosen in order to obtain a GdFe alloy magnetization dominated by the rare-earth moments and a TbFe magnetization dominated by iron (the magnetization is along that of Fe)[24] as sketched on Fig. 1. As a consequence, the resulting interface coupling, dominated by the Fe/Fe ferromagnetic exchange interactions, is antiferromagnetic between the magnetization densities of each layer.

$Gd_{40}Fe_{60}$ and $Tb_{12}Fe_{88}$ alloys were prepared by coevaporation of the pure elements from three different crucibles in a high-vacuum chamber as described elsewhere. The deposition rates were monitored by quartz oscillating systems, previously calibrated by optical methods. The substrates (glass) were kept at 77 K in order to obtain amorphous alloys. The pressure was in the $10^{-8}$ mbar range during the coevaporation. The compositions of the alloys were checked by x-ray analysis and were found within 2% to 4% off the nominal values. The amorphicity of the alloys has been checked by transmission electron microscopy. The mean roughness of a 20-nm-thick GdFe layer determined *ex situ* by atomic-force microscopy is around 0.4 nm. A 30-nm capping Si layer is deposited to form a glass$\|Tb_{12}Fe_{88}$ (50 nm)/$Gd_{40}Fe_{60}$ (100 nm)/Si (30 nm) which was used to perform magnetization measurements. Due to the growth geometry an in-plane uniaxial anisotropy axis was induced in the GdFe alloy as it is clearly shown in Refs. 25 and 26. Following the Stoner-Wohlfarth model of uniform rotation[27] the anisotropy constant is given by $K=\frac{M_S H_K}{2}$, where $M_S^{GdFe}=500\pm100$ emu/cm$^3$ is the magnetization and $H_K^{GdFe}=100\pm10$ Oe is the anisotropy field deduced from the magnetization loop of a 100-nm-thick $Gd_{40}Fe_{60}$ layer at $T=300$ K. The anisotropy constant is then equal to $K_{GdFe}=(2.5\pm1)\times10^4$ erg/cm$^3$ at $T=300$ K. With the same procedure $K_{TbFe}=(2.5\pm1)\times10^4$ erg/cm$^3$ with $M_S^{TbFe}=225\pm50$ emu/cm$^3$ and $H_K^{TbFe}=250\pm50$ Oe. The exchange stiffness $A$ is obtained from the Mimura relation.[28] For an alloy it takes into account the spin value, the interatomic distances, and the exchange integrals of each element. With the exchange integrals and spin values from Ref. 28: $S_{Fe}=1$ and $S_{Gd}=7/2$, we find $A_{GdFe}=(6\pm2)\times10^{-7}$ erg/cm. For $Tb_{12}Fe_{88}$ the exchange stiffness could be evaluated to $A_{TbFe}=15\times10^{-8}$ erg/cm.

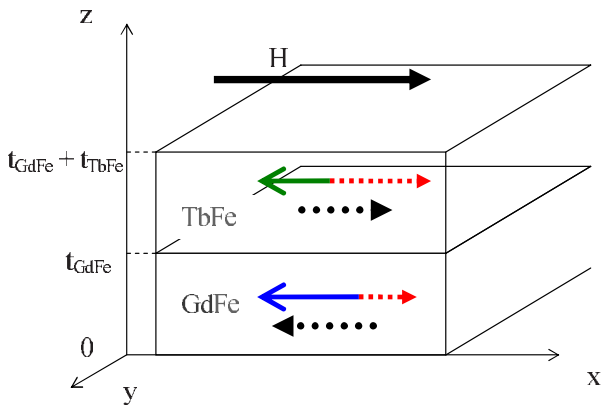


FIG. 1. (Color online) Schematic of the $Tb_{12}Fe_{88}$(50 nm)/$Gd_{40}Fe_{60}$(100 nm) bilayer. Arrows with green and blue lines represent, respectively, Tb and Gd sublattice magnetizations, arrows with red dash lines represent the Fe sublattice magnetization, and the black arrow with dots line represent the net magnetization of the alloy.

### B. Transverse and longitudinal magnetization measurements

Longitudinal ($M_\|$ along $Ox$ as defined in Fig. 1) and transverse magnetization components ($M_\perp$ along $Oy$ as defined in Fig. 1) were measured as a function of the magnetic field by using a custom-built alternating gradient force magnetometer.[29] The sample was mounted on a quartz cantilever attached to one end of a piezoelectric bimorph. Two sets of orthogonal Helmholtz coils were used to generate an alternating field gradient, whose direction could be tuned within the $xy$ plane. This field gradient generates a force on the sample which is proportional to the sample's magnetiza-

TABLE I. Magnetic parameters concerning the GdFe and the TbFe layers used to perform the micromagnetic simulations.

| | GdFe layer | TbFe Layer |
|---|---|---|
| Thickness | $t_{GdFe}=100$ nm | $t_{TbFe}=50$ nm |
| Magnetization | $M_S^{GdFe}=500$ emu/cm$^3$ | $M_S^{TbFe}=225$ emu/cm$^3$ |
| Anisotropy field | $H_K^{GdFe}=100$ Oe | $H_K^{TbFe}=250$ Oe |
| Exchange stiffness | $A_{GdFe}=6\times10^{-7}$ erg/cm | $A_{TbFe}=8\times10^{-8}$ erg/cm |
| Thickness /exchange length | $t_{GdFe}/\lambda_{GdFe}\approx2$ | $t_{TbFe}/\lambda_{TbFe}\approx3$ |
| Interface exchange coupling | $J=-1$ erg/cm$^2$ | |

tion. When the ac field gradient frequency is tuned to the resonance of the quartz cantilever, the magnetic force induces mechanical oscillations which in turn generate an ac voltage on the sides of the piezoelectric bimorph. By rotating both sample's easy axis and the field gradient direction with respect to the applied magnetic field, both longitudinal and transverse magnetization components can be measured for any magnetic field direction (see Fig. 4).

### C. Unidimensional micromagnetic calculation

To understand the evolutions of the magnetic configurations, we proceeded to a one-dimensional calculation of the magnetic profile. Due to the demagnetizing field, the magnetization is kept in the plane of the layers and the magnetic profile is characterized by a single-depth-dependent angle $\theta(z)$ referenced to the anisotropy direction. The magnetic surface energy of the bilayer is calculated by considering, for each layer (GdFe and TbFe): the exchange energies, the uniaxial anisotropy energies, the Zeeman energy, and the interface exchange energy.

$$E=\int_0^{t_{GdFe}}\left\{A_{GdFe}\left[\frac{d\theta(z)}{dz}\right]^2+K_{GdFe}\sin^2\theta(z)-HM_{GdFe}\cos[\theta(z)-\psi]\right\}dz+\int_{t_{GdFe}}^{t_{GdFe}+t_{TbFe}}\left\{A_{TbFe}\left[\frac{d\theta(z)}{dz}\right]^2+K_{TbFe}\sin^2\theta(z)-HM_{TbFe}\cos[\theta(z)-\psi]\right\}dz-J\cos(\theta_{TbFe}^i-\theta_{GdFe}^i) \tag{1}$$

with $\psi$ the angle between the in-plane external field **H** and the GdFe easy axis ($Ox$), and where $\theta_{GdFe}^i$ and $\theta_{TbFe}^i$ are, respectively, the angle of the magnetization at the interface in GdFe and in the TbFe layer (measured from $Ox$). $t_{GdFe}$ and $t_{TbFe}$ are, respectively, the GdFe and TbFe layer's thickness and the total thickness is defined as $t=t_{GdFe}+t_{TbFe}$. To determine the possible energy minima, Eq. (1) were transformed in a discrete form so that the bilayer is modeled a 150 spins chain. Different initial conditions are used in order to determine all the local minima of energy. Depending on the applied field, we reached one, two or three minima, only one of them corresponding to the absolute minimum (stable configuration) the other ones being local minima (metastable configurations). The magnetic parameters used to describe the GdFe and TbFe layers are reported in Table I. Those parameters are found to be in the error bars of the one determined in the Sec. I.

The stable and metastable magnetization profiles are presented in a polar plot (Fig. 3) each point of this circular plot being representative of the orientation of the magnetization of a slab of the sample. The radius $r$ at which the point stands represents it's position in the layer thickness. The point located at the center of the circle represents the first slab (the outer one) of the GdFe layer. The second point represents the second slab and so on, up to the point which reaches the inner circle which represents the last GdFe slab, which is at the interface between the GdFe and TbFe layers. Indeed, this inner circle represents the boundary between the two materials. The set of points between this inner circle and the outer circle represent the magnetization of TbFe slabs. The information about the orientation of the magnetization of each slab of material is given by the angular positions $\theta$ of its representative point, which give simply the orientation of the spin in reference to the $Ox$ easy-axis direction, the field orientation being at an angle $\psi$ from this direction. We recall as $\theta_{GdFe}^0$ the angular position of the central point (first GdFe slab), $\theta_{GdFe}^i$ the angular position of the internal point at the interface (interface GdFe slab), $\theta_{TbFe}^i$ the angular position of the external point at the interface (interface TbFe slab), and finally $\theta_{TbFe}^l$ the point located on the external circle and corresponding to the outer TbFe slab.

In order to compare numerical simulations with magnetization measurements, the longitudinal ($M_\parallel$) and transverse ($M_\perp$) magnetization of the energies minima profiles were calculated using

$$M_\parallel=\int_0^{t_{GdFe}}(M_{GdFe}\cos[\theta(z)-\psi])dz+\int_{t_{GdFe}}^{t_{GdFe}+t_{TbFe}}(M_{TbFe}\cos[\theta(z)-\psi])dz, \tag{2}$$

$$M_\perp=\int_0^{t_{GdFe}}(M_{GdFe}\sin[\theta(z)-\psi])dz+\int_{t_{GdFe}}^{t_{GdFe}+t_{TbFe}}(M_{TbFe}\sin[\theta(z)-\psi])dz. \tag{3}$$

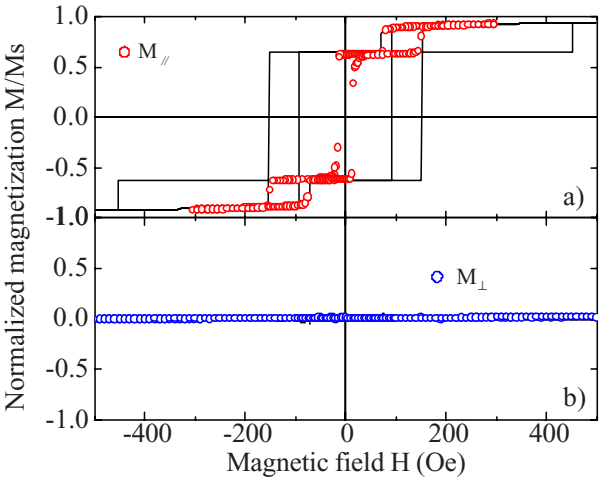


FIG. 2. (Color online) Normalized (a) longitudinal $M_{\parallel}$ and (b) transverse $M_{\perp}$ component of the magnetization (open symbols) as a function field compared to the results of the micromagnetic calculation (lines).

## III. EXPERIMENTAL RESULTS AND DESCRIPTION OF THE MAGNETIC STRUCTURES

### A. Magnetization along the easy axis

In order to understand the magnetic behavior of the sample for $\psi=0°$, i.e., when the field is always applied along the easy axis, the experimental data will first be qualitatively described and analyzed. Then the results of the calculation will be analyzed and finally compared with the experiments.

Figure 2 shows the behavior of the longitudinal ($M_{\parallel}$) and transverse ($M_{\perp}$) magnetization components. In this geometry, we did not measure any significant transverse magnetization [Fig. 2(b)]. However $M_{\parallel}$ [Fig. 2(a)] exhibits three well-defined minor loops with rather sharp steps: a central loop ($c$ loop) and two symmetrical side loops ($s$ loops) which in fact are the same one reproduced in positive and negative fields. The magnetic configurations and the consequential $M_{\parallel}$, $M_{\perp}$ values result from the competition between the Zeeman energy which tends to align both magnetizations along the field direction and the antiferromagnetic interface exchange coupling which lead to an antiparallel (AP) alignment of the two magnetizations. On the light of this energy competition one may qualitatively explain some of the experimental results. For very large applied field the two magnetizations are expected to be parallel (maximum $M_{\parallel}$ and minimum $M_{\perp}$). However to minimize the interface exchange interaction an interface magnetic domain wall (iDW) may be created.[30] The iDW thickness is expected to increase as the field decreases. This effect has been named domain-wall decompression.[31] The presence of an iDW implies the existence of magnetic moment with a component perpendicular to the field which results in a decrease in $M_{\parallel}$. The smooth $M_{\parallel}$ decreasing may then be explained by this iDW compression effect.[31] For a certain field the iDW energy is larger than the Zeeman energy gain and the magnetization reversal of one of the layer toward the field is expected. This is clearly evidenced by the magnetization jump observed on the $M_{\parallel}$ versus field curve. The consequence of this magnetization reversal is the annihilation of the iDW. While the two alloys magnetizations are antiparallel, the total magnetization stays constant. Then for a small negative field a large magnetization drop is observed which results from the reversal of the two alloys magnetizations. The description of the measurement may be continued using symmetry argument. Measurements of the anisotropic magnetoresistance on similar sample[30] are consistent with the above conclusions.

We can notice the flatness of the magnetization in the central magnetic stages. On the opposite, the (external) upper and lower magnetization stages are rounded, which means that coming from high field, the magnetization profile evolves before reaching the first step. This type of magnetization reversal was first observed for GdFe/FeSn systems.[30]

From the micromagnetic calculation we could deduce the different magnetic configurations for various magnetic fields with $\psi=0°$ and the field dependence of those magnetic configuration energies as shown in Fig. 3. For $H=500$ Oe two totally equivalent configurations may be reached by the simulation which is consistent with the fact that the field is applied along a symmetry direction. In Fig. 3(b) the two configurations are presented and no other metastable solution is found. Only one of the two configurations is described in details in the following. Starting from the center of the circular plot the magnetization of GdFe is in the field direction ($\theta^0_{\mathrm{GdFe}}=0°$). Then $\theta$ exhibits a progressive departure from 0° and reaches $\theta^i_{\mathrm{GdFe}}=336°$ at the GdFe/TbFe interface. Then the next point, located beyond the interface and corresponding to the first (inner) TbFe layer makes approximately a −180° angle with the previous one which is the consequence of the antiferromagnetic coupling between the GdFe and TbFe alloys ($\theta^i_{\mathrm{TbFe}}=145°$). Then, moving in the TbFe layer, the magnetization rotates progressively and rapidly to the field direction to reach almost 0° ($\theta^f_{\mathrm{TbFe}}=2°$). This configuration is characterized by a twist of the magnetization (domain wall) mainly located in the TbFe layer. This configuration will be named domain-wall configuration. It occurs because of the antiferromagnetic interface coupling and is located mostly in TbFe because the domain-wall energy is lower if it is located in the TbFe rather that in the GdFe. Indeed the interface domain-wall energy under an applied field $H$ can be approximated by by $\sigma=4\sqrt{A(K+2M_sH)}$ (Ref. 7) and the magnetization of GdFe is larger than that of TbFe whereas the exchange stiffness of TbFe ($A_{\mathrm{TbFe}}$) is lower than the one for GdFe($A_{\mathrm{GdFe}}$). As already mentioned there are two energetically equivalent configurations: one for which the magnetization from the interface to the outer TbFe surface rotates clockwise (cw-DW) and the other one counterclockwise (ccw-DW).[21,32]

The calculations performed for $H=200$ Oe lead to two nonequivalent solutions: a stable solution and a metastable one [Figs. 3(a) and 3(c)]. The stable solutions are the two DW configurations very similar to that obtained for $H=500$ Oe except that the twist spread over more slabs and the outer TbFe is now far from zero ($\theta^f_{\mathrm{TbFe}}=10°$). Indeed the Zeeman energy is weakened and the exchange coupling tends to minimize the angle between two magnetization slabs. The metastable solution corresponds to the configuration in which the GdFe magnetization is uniformly aligned

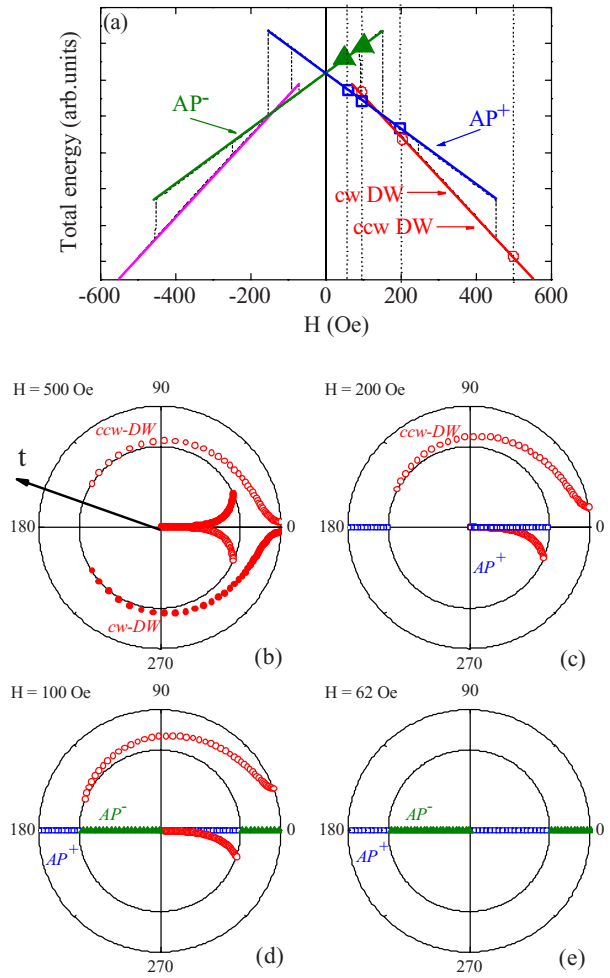


FIG. 3. (Color online) (a) Variation in the total energy given by [Eq. (1)] as a function of the magnetic field applied along the easy-axis direction ($\psi$=0°). The full line is the energy minima corresponding to a domain-wall state. The dash line is the energy minima corresponding to an antiparallel alignment ($AP^+$) of the two layers magnetization. The dot line is the energy minima corresponding to an antiparallel alignment ($AP^-$) of the two layers magnetization. The symbols refer to the magnetic-configuration sketch on (a)–(d). [(a)–(d)] Polar plots of the depth dependence of the magnetization angle as obtained from the magnetic configuration. The calculation was carried out using the parameters gathered in Table I with the field applied along the easy axis [($\psi$=0°) for four different fields (a) $H$=500 Oe, (b) 200 Oe, (c) 100 Oe, and (d) 62 Oe].

along the field direction ($Ox$) and the TbFe magnetization is antiparallel to it. This configuration for which the two alloys magnetizations are antiparallel and the net bilayer magnetization is parallel to $Ox$ will be called $AP^+$.

For $H$=100 Oe three solutions are obtained [Figs. 3(a) and 3(d)]: the two solutions previously described and a configuration for which the two alloys magnetizations are antiparallel but the net bilayer magnetization is antiparallel to $Ox$($AP^-$). The DW solution is a larger domain wall and $\theta^t_{\mathrm{TbFe}}$ and $\theta^i_{\mathrm{TbFe}}$ keep on increasing. However as shown in Fig. 3(a) the DW energy crosses the $AP^+$ energy for $H$=150 Oe. This means that for fields lower than 150 Oe the DW configuration is now a metastable state and $AP^+$ a stable one but that an energy barrier has to be crossed to drop from one state to the other.

For $H$=62 Oe [Fig. 3(e)], there are only two solutions left and both correspond to antiparallel aligned configurations ($AP^+$ and $AP^-$). Indeed for $H<67$ Oe the DW state disappears and $AP^+$ and $AP^-$ are the two possible configurations. $AP^+$ is the stable state in positive field and switch to metastable as soon as the field changes sign.

As the occurrence of one or of the other solution depends on the history of the experiment process calculated and measured magnetization values have to be compared. The calculated and experimental $M_{\parallel}$ values are show in Fig. 2. It is clear that the upper and lower stages correspond to DW configuration. These stages are not flat because of the evolution of the width of the domain wall which appears to become larger as the field is decreased, which lower the net magnetization. The intermediate stages corresponding to the $AP^+$ and $AP^-$ configurations are perfectly flat. Finally, the $s$ loops correspond to transitions between DW and antiparallel configuration and the $c$ loop is a switch between $AP^+$ and $AP^-$. It is to notice that the calculations reproduce perfectly the amplitudes of the step and the evolution of the magnetization in the different stages. There is always one of the stable or metastable solutions which fit perfectly the data. The calculation gives the possible solution but cannot predict the field at which the transition takes places however it gives the upper and lower field limits of the transitions.

For $\psi$=0°, from the calculation we find that the net perpendicular magnetization of each configuration is close to zero as experimentally observed. In that case $M_{\perp}$ measurements do not give new information on the magnetic profile. Due to the system symmetry, two symmetrical and equivalent solutions are always possible. Since the two configurations have the same $M_{\parallel}$ it was not possible to state neither that only one configuration nor that both of them are present (forming domains).

### B. Magnetization with $\psi \neq 0°$

The results of the measurements of the magnetizations $M_{\parallel}$ and $M_{\perp}$ performed for the angular rotations $\psi$=30°, 45°, 60°, and 90° are shown in Fig. 4. The two main features exhibited by these curves are a progressive evolution of $M_{\parallel}$ and the occurrence of a significant transverse component $M_{\perp}$. In a general way, $M_{\parallel}$ still exhibits the three minor loops but the intermediate stages are less and less flat and the general shape of the cycle is more and more rounded when $\psi$ is increased. $M_{\perp}$ has a significant value especially at the vicinity of zero field.

As is it shown in Fig. 4, the calculated $M_{\parallel}$ and $M_{\perp}$ magnetizations follow satisfactory the experimental results, in the sense that there is always a solution which follows the experimental data and the amplitude of the transition are perfectly reproduced. As an example, we present and comment in Fig. 5 the configurations found from simulations and the evolution of the corresponding energy for $\psi$=45°.

For the field larger than $H$=200 Oe [Fig. 5(b)] two nonequivalent solutions are found and both are of the cw-DW

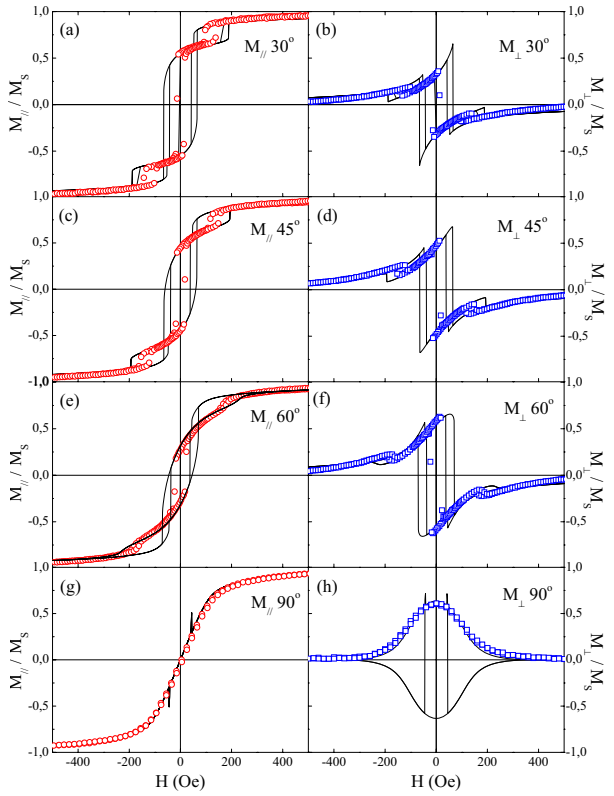


FIG. 4. (Color online) Normalized longitudinal $M_{\|}$ component of the magnetization as a function field (a) at 30°, (c) at 45°, (e) at 60°, and (g) at 90°, from the easy-axis magnetization, respectively, and transverse $M_{\perp}$ component of the magnetization as a function field (b) at 30° (d) at 45° (f) at 60° and (h) at 90°. In each graphic the experimental data $M_{\|}$ (red open circles) and $M_{\perp}$ (blue open square) are compared to the results of the micromagnetic calculation (lines).

type. The magnetization of the outer GdFe slabs are along directions between the field direction (45°) and that of the easy axis 0° with $\theta^0_{\mathrm{GdFe}}=30°$ for the cw-DW type and $\theta^0_{\mathrm{GdFe}}=35°$ for the ccw-DW type. The GdFe moments leave progressively their initial directions $\theta^0_{\mathrm{GdFe}}$ and turn, respectively, clockwise and counterclockwise in the plot circle to reach $\theta^i_{\mathrm{GdFe}}=10°$ and 60°, respectively. At the interface $\theta$ exhibits a 180° step and the TbFe magnetization rotates up to external directions located again between the field direction and the easy axis with $\theta^i_{\mathrm{TbFe}}=48°$ for the cw-DW type and $\theta^i_{\mathrm{TbFe}}=12°$ for the ccw-Dw type. It is to note that the cw-DW type and ccw-DW type give nearly the same contributions to $M_{\|}$ and $M_{\perp}$ with a slight lower energy for the cw-DW type.

At $H=100$ Oe [Fig. 5(c)], the ccw-DW type occurs again but the cw-DW type disappears for an $AP^+$ type configuration. As shown in Fig. 5(a) the energy of $AP^+$ type configuration is lower than the DW one at this field, we observed one or the other configuration according to the sample magnetic history. The *s* loop originates from the transition from ccw-DW type to the $AP^+$ type. The transition provides a simultaneous reduction in $M_{\|}$ and $M_{\perp}$. The *s* loops are thus the results of the same kind of transition as for $\psi=0$ except

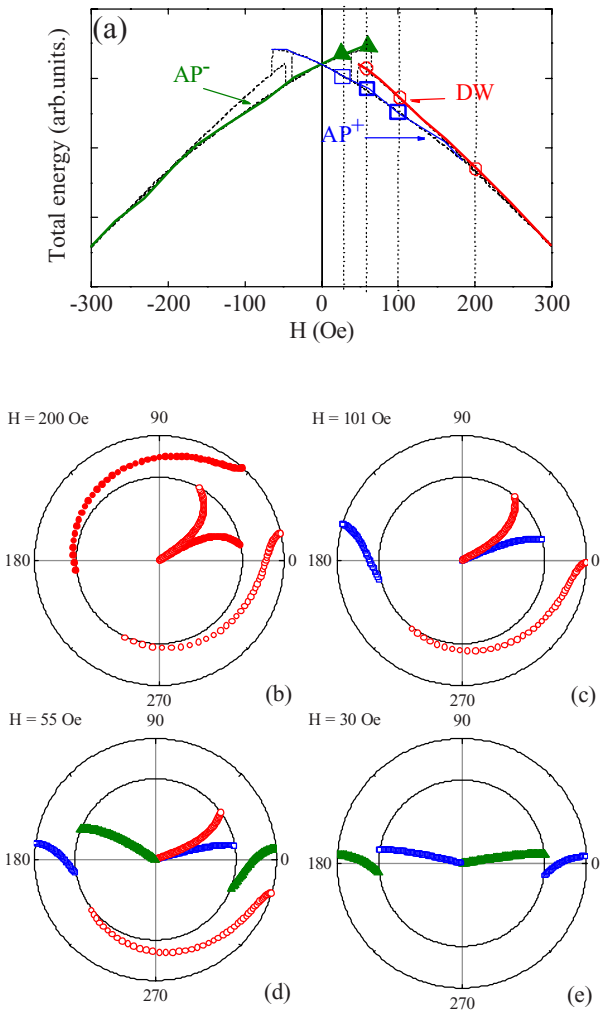


FIG. 5. (Color online) (a) Variation in the total energy given by [Eq. (1)] as a function of the magnetic field applied 45° away from the easy-axis direction ($\psi=45°$). The full line is the energy minima corresponding to a domain-wall state. The dash line is the energy minima corresponding to an antiparallel alignment ($AP^+$) of the two layers magnetization. The dot line is the energy minima corresponding to an antiparallel alignment ($AP^-$) of the two layers magnetization. The symbol refer to the magnetic-configuration sketch on (a)–(d). [(a)–(d)] Polar plots of the depth dependence of the magnetization angle as obtained from the magnetic configuration. The calculation was carried out using the parameters gathered in Table I with the field applied along the easy axis [($\psi=45°$) for four different fields (a) $H=200$, (b) 101, (c) 55, and (d) 30 Oe].

that the $AP^+$ and $AP^-$ configurations are more and more twisted as $\psi$ increases.

At $H=55$ Oe [Fig. 5(d)], a new solution occurs besides those observed at 100 Oe. It is an $AP^-$ configuration. Because of the lower field, the magnetizations in both layers are closer and closer to the easy axis and as a consequence, $M_{\perp}$ becomes larger. The $AP^+$ type is still more stable than the DW-type configuration [Fig. 5(a)].

Finally at $H=30$ Oe [Fig. 5(e)], only the AP configuration remain possible and it is clear that the central loop is a

switch between these configurations. The stages between the *c* loop and the *s* loops are no longer flat because the aligned-type configurations are more and more twisted and that this twist is very sensitive to the field.

The configurations are very similar for the other $\psi$ angle. It is remarkable that in all cases, the data always correspond to one of the calculated configurations and that the amplitudes of the drops are very well predicted which strongly support the micromagnetic calculation.

### C. Configuration $\psi$=90°

The longitudinal magnetization loop becomes very smooth without any apparent transition [Figs. 4(g) and 4(h)]. On the other hand, the transverse magnetization reaches its maximum value for this $\psi$=90° angle in zero field. As a matter of fact, following the field rotation of the sample from $\psi$=0° prior the magnetization measurements, the transverse component never changes its sign.

The simulations performed in this geometrical situation are shown in Fig. 6 and as a result of the symmetry, we found at each field two equivalent solutions, one clockwise, the second one counterclockwise. For a 200 Oe field, the calculated configuration for the cw-DW type is obtained with $\theta^0_{\mathrm{GdFe}}$=99°, $\theta^i_{\mathrm{GdFe}}$=125°, $\theta^i_{\mathrm{TbFe}}$=310°, and $\theta^t_{\mathrm{TbFe}}$=35°. For larger field (not shown) this configuration is clearly dominated by the field which leads to $\theta^0_{\mathrm{GdFe}}$ and $\theta^t_{\mathrm{TbFe}}$ almost in the field direction. Under a low field where the configuration is dominated by the anisotropy direction, the structure is of the aligned type (see $H$=14 Oe) and it is a perfect aligned state with $H$=0, which leads to $M_{\parallel}$=0 and $M_{\perp}$ maximum. The configuration changes continuously between these values and there is no abrupt transition between these two types of magnetic structures. The sign of $M_{\perp}$ never changes and is always positive because the sample has been first rotated from $\psi$=0° under field, which lead to a ccw-DW type in positive field and a clockwise one in negative field. There is no switch between two aligned-type configurations and then no change in $M_{\perp}$ sign. It is to note again how accurate the results of the calculation are when compared to the experimental data.

## IV. CONCLUSIONS

An antiferromagnetically exchange-coupled GdFe/TbFe bilayer system which exhibits exchange bias at low temperature has been studied. By measuring the sample at room temperature our aim was to deduce the magnetic configuration developing as function of field orientation and amplitude. Both $M_{\parallel}$ and $M_{\perp}$ were measured and then compared to the results of a micromagnetic with a calculation with no adjustable parameters. The calculation allows obtaining the possible magnetic configurations but it does not predict the field at which the system switches from one configuration to the other. It is remarkable to observe that in all cases, experimental data are always in agreement with one of the calculated magnetic configurations and that the amplitudes of the drops are very well predicted. From the field range at which the two magnetic configurations coexist we can deduce accurately the field range at which reversal may occur.

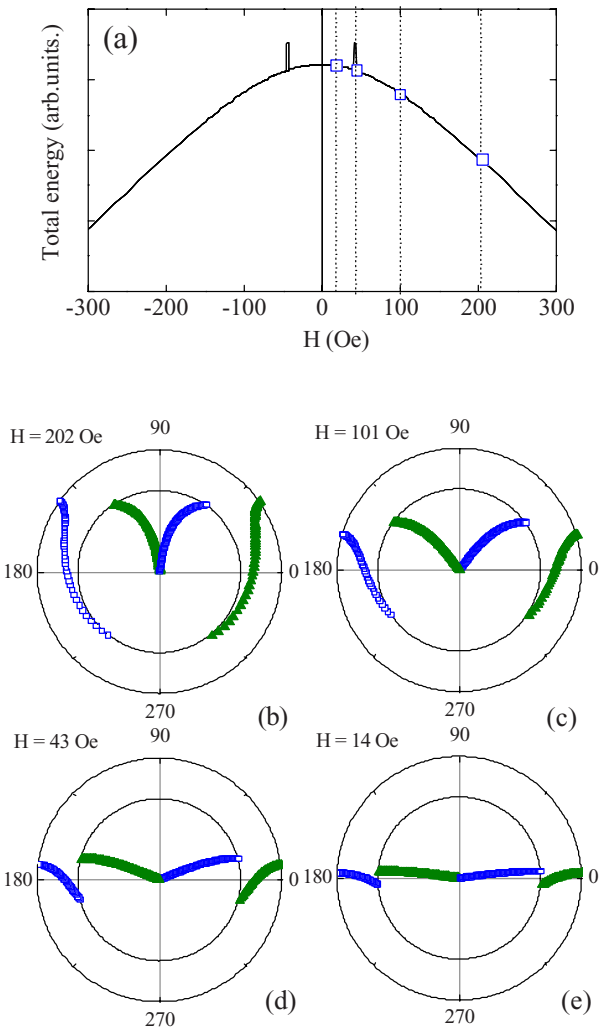


FIG. 6. (Color online) (a) Variation in the total energy given by [Eq. (1)] as a function of the magnetic field applied along the hard-axis direction ($\psi$=90°). Only one energy minima is obtained except for $H$=43 Oe it corresponds to two symmetrical magnetic configurations. The symbol refer to the magnetic-configuration sketch on (a)–(d). [(a)-(d)] Polar plots of the depth dependence of the magnetization angle as obtained from the magnetic configuration. The calculation was carried out using the parameters gathered in Table I with the field applied along the easy axis [($\psi$=45°) for four different fields (a) $H$=202, (b) 101, (c) 43, and (d) 14 Oe].

The magnetic configuration inside the bilayer system and its evolution with field was obtained for different field orientation. We observed mainly two types of structures: the interface domain wall which can show two different chiralities (cw-DW and ccw-DW) and the antiparallel configurations ($AP^+$ and $AP^-$) ones. The interface domain wall was mainly located in the very iron-rich TbFe because at room temperature its exchange stiffness is weak and its magnetization density is smaller than that of GdFe. The GdFe magnetization aligns as much as possible in the field direction to lower the Zeeman energy. For an applied field away from the hard-axis

magnetization the domain-wall states and the antiparallel-type state may be well distinguished and an irreversible transition occurs between the two states. However for an applied field along the hard axis the two types of configurations cannot be distinguished anymore and no transition is observed. The hysteresis loop is fully reversible.

The knowledge of the interface magnetic configurations is of prime importance to understand and to tune the exchange-bias field at low temperature. Indeed it was shown in Ref. 17 that the interface configuration inside the TbFe is frozen as the sample is cooled down because the anisotropy of TbFe rises quickly as the temperature decreases. The present study allows understanding the complex angular dependence of systems cooled in noncollinear configurations and the related strong dependence of the exchange bias on the cooling-field orientation and amplitude.[18,33]

## ACKNOWLEDGMENTS

The authors thank D. Pierre and S. Suire, for help with the sample preparation and Eric E. Fullerton and M. Hehn for fruitful discussion.

*stephane.mangin@lpm.u-nancy.fr

[1] J. R. Childress, M. J. Carey, R. J. Wilson, N. Smith, C. Tsang, M. K. Ho, K. Carey, S. A. MacDonald, L. M. Ingall, and B. A. Gurney, IEEE Trans. Magn. **37**, 1745 (2001).
[2] W. H. Meiklejohn and C. P. Bean, Phys. Rev. **105**, 904 (1957).
[3] A. E. Berkowitz and K. Takano, J. Magn. Magn. Mater. **200**, 552 (1999).
[4] J. Nogues and I. K. Schuller, J. Magn. Magn. Mater. **192**, 203 (1999).
[5] Miguel Kiwi, J. Magn. Magn. Mater. **234**, 584 (2001).
[6] E. E. Fullerton, J. S. Jiang, M. Grimsditch, C. H. Sowers, and S. D. Bader, Phys. Rev. B **58**, 12193 (1998).
[7] S. Mangin, G. Marchal, and B. Barbara, Phys. Rev. Lett. **82**, 4336 (1999).
[8] J. Nogues, D. Lederman, T. J. Moran, and Ivan K. Schuller, Phys. Rev. Lett. **76**, 4624 (1996).
[9] J. Nogues, C. Leighton, and Ivan K. Schuller, Phys. Rev. B **61**, 1315 (2000).
[10] C. Leighton, M. R. Fitzsimmons, A. Hoffmann, J. Dura, C. F. Majkrzak, M. S. Lund, and Ivan K. Schuller, Phys. Rev. B **65**, 064403 (2002).
[11] W. A. A. Macedo, B. Sahoo, J. Eisenmenger, M. D. Martins, W. Keune, V. Kuncser, R. Rohlsberger, O. Leupold, R. Rüffer, J. Nogues, Kai Liu, K. Schlage, and Ivan K. Schuller, Phys. Rev. B **78**, 224401 (2008).
[12] R. Morales, Zhi-Pan Li, J. Olamit, Kai Liu, J. M. Alameda, and Ivan K. Schuller, Phys. Rev. Lett. **102**, 097201 (2009).
[13] M. R. Fitzsimmons, C. Dufour, K. Dumesnil Jian Dou, and Michael Pechan, Phys. Rev. B **79**, 144425 (2009).
[14] T. L. Kirk, O. Hellwig, and E. E. Fullerton, Phys. Rev. B **65**, 224426 (2002).
[15] M. R. Fitzsimmons, S. Park, K. Dumesnil, C. Dufour, R. Pynn, J. A. Borchers, J. J. Rhyne, and Ph. Mangin, Phys. Rev. B **73**, 134413 (2006).
[16] K. Dumesnil, C. Dufour, S. Fernandez, M. Oudich, A. Avisou, A. Rogalev, and F. Wilhelm, J. Phys.: Condens. Matter **21**, 236002 (2009).
[17] S. Mangin, F. Montaigne, and A. Schuhl, Phys. Rev. B **68**, 140404(R) (2003).
[18] S. Mangin, T. Hauet, Y. Henry, F. Montaigne, and Eric E. Fullerton, Phys. Rev. B **74**, 024414 (2006).
[19] Y. Henry, S. Mangin, T. Hauet, and F. Montaigne, Phys. Rev. B **73**, 134420 (2006).
[20] T. Hauet, J. A. Borchers, Ph. Mangin, Y. Henry, and S. Mangin, Phys. Rev. Lett. **96**, 067207 (2006).
[21] J. McCord, Y. Henry, T. Hauet, F. Montaigne, Eric E. Fullerton, and S. Mangin, Phys. Rev. B **78**, 094417 (2008).
[22] T. Hauet, S. Mangin, J. McCord, F. Montaigne, and Eric E. Fullerton, Phys. Rev. B **76**, 144423 (2007).
[23] R. W. Cochrane, R. Harris, and M. J. Zuckermann, Phys. Rep. **48**, 1 (1978).
[24] P. Hansen, C. Clausen, G. Much, M. Rosenkranz, and K. Witter, J. Appl. Phys. **66**, 756 (1989).
[25] S. Mangin, C. Bellouard, G. Marchal, and B. Barbara, J. Magn. Magn. Mater. **165**, 161 (1997).
[26] F. Montaigne, S. Mangin, and Y. Henry, Phys. Rev. B **67**, 144412 (2003).
[27] E. C. Stoner and E. P. Wohlfarth, Philos. Trans. R. Soc. London, Ser. A **240**, 599 (1948).
[28] Y. Mimura, N. Imamura, T. Kobayashi, A. Okada, and Y. Kushiro, J. Appl. Phys. **49**, 1208 (1978).
[29] L. Thomas, A. Rahmani, P. Renaudin, and A. Wack, J. Appl. Phys. **93**, 7062 (2003).
[30] F. Canet, S. Mangin, C. Bellouard, and M. Piecuch, Europhys. Lett. **52**, 594 (2000); F. Canet, C. Bellouard, S. Mangin, C. Chatelain, and M. Piecuch, Eur. Phys. J. B **34**, 381 (2003).
[31] S. Mangin, G. Marchal, C. Bellouard, W. Wernsdorfer, and B. Barbara, Phys. Rev. B **58**, 2748 (1998).
[32] Y. Henry, S. Mangin, and F. Montaigne, Phys. Rev. B **69**, 140401(R) (2004).
[33] E. Jimenez, J. Camarero, J. Sort, J. Nogues, A. Hoffmann, F. J. Teran, P. Perna, J. M. Garcia-Martin, B. Dieny, and R. Miranda, Appl. Phys. Lett. **95**, 122508 (2009).